Published for SISSA by Springer

Received: May 2, 2013
Revised: July 2, 2013
Accepted: August 8, 2013
Published: September 2, 2013

Physics performance for scalar electron, scalar muon and scalar neutrino searches at $\sqrt{s} = 3$ TeV and 1.4 TeV at CLIC

M. Battaglia,[a,b] **J-J. Blaising,**[c] **J.S. Marshall,**[d] **S. Poss,**[a,c] **A. Sailer,**[a] **M. Thomson**[d] **and E. van der Kraaij**[a]

[a] *CERN, CH-1211 Geneva, Switzerland*
[b] *Santa Cruz Institute of Particle Physics, University of California, Santa Cruz, CA 95064, USA*
[c] *Laboratoire d'Annecy-le-Vieux de Physique des Particules, Annecy-le-Vieux, France*
[d] *Cavendish Laboratory, University of Cambridge, Cambridge, U.K.*

E-mail: Marco.Battaglia@cern.ch, Jean-Jacques.Blaising@cern.ch, marshall@hep.phy.cam.ac.uk, stephane.guillaume.poss@cern.ch, thomson@hep.phy.cam.ac.uk, andre.philippe.sailer@cern.ch, Erik.Van.Der.Kraaij@cern.ch

Abstract: The determination of scalar lepton and gaugino masses is an important part of the programme of spectroscopic studies of Supersymmetry at a high energy e^+e^- linear collider. In this article we present results of a study of the processes: $e^+e^- \to \tilde{e}^+_R\, \tilde{e}^-_R \to e^+e^-\ \tilde{\chi}^0_1\ \tilde{\chi}^0_1$, $e^+e^- \to \tilde{\mu}^+_R\, \tilde{\mu}^-_R \to \mu^+\mu^-\ \tilde{\chi}^0_1\ \tilde{\chi}^0_1$, $e^+e^- \to \tilde{e}^+_L\, \tilde{e}^-_L \to e^+\ e^-\ \tilde{\chi}^0_2\ \tilde{\chi}^0_2$ and $e^+e^- \to \tilde{\nu}_e\, \tilde{\nu}_e \to e^+\ e^-\ \tilde{\chi}^+_1\ \tilde{\chi}^-_1$ in two Supersymmetric benchmark scenarios at $\sqrt{s} =$ 3 TeV and 1.4 TeV at CLIC. We characterize the detector performance, lepton energy resolution and boson mass resolution. We report the accuracy of the production cross section measurements and the $\tilde{e}_R$, $\tilde{\mu}_R$, $\tilde{\nu}_e$, $\tilde{\chi}^\pm_1$, and $\tilde{\chi}^0_1$ mass determinations, estimate the systematic errors affecting the mass measurement and discuss the requirements on the detector time stamping capability and beam polarization. The analysis accounts for the CLIC beam energy spectrum and the dominant beam-induced background. The detector performances are incorporated by full simulation and reconstruction of the events within the framework of the CLIC_ILD_CDR detector concept.

Keywords: Supersymmetry, e+-e- Experiments

ArXiv ePrint: 1304.2825

doi:10.1007/JHEP09(2013)001

JHEP09(2013)001

Contents

1 Introduction 1

2 Event simulation 3

3 Event reconstruction 4
- 3.1 Two lepton final states 5
- 3.2 Two leptons and four jets final states 6
- 3.3 Reconstruction with beam-induced Background 7

4 Event selection 12

5 Slepton and gaugino mass determination 13

6 Systematic uncertainty related to the event selection 17

7 Systematic uncertainty related to the luminosity spectrum 19

8 Polarization 20

9 Summary 21

JHEP09(2013)001

1 Introduction

One of the main objectives of linear collider experiments is the precision spectroscopy of new particles predicted in theories of physics beyond the Standard Model (SM), such as Supersymmetry (SUSY) [1–5]. In this article, we study the production of the supersymmetric partners of the muon, electron and neutrino in two specific SUSY benchmark points, where we assume R-parity conservation within the so-called constrained Minimal Supersymmetric extension of the SM (cMSSM). In this model the neutralino ($\tilde{\chi}_1^0$) is the lightest supersymmetric particle. Table 1 shows the masses and the branching ratios of the supersymmetric particles for the two benchmark points P1 and P2. The squarks masses $\tilde{u}_R, \tilde{u}_L, \tilde{d}_R, \tilde{d}_L$ are 1.9 TeV for P1 and 2.2 TeV for P2. The parameters of the two benchmark points are such that they are compatible with the constraints of other observables, e.g. Ω_{DM}, $\Delta(g-2)_\mu$, $BR(b \to s\gamma)$ and with LHC limits on squarks and gluinos. The benchmark points mass spectrum were chose before the 125 GeV boson discovery was made. For both benchmark points the Higgs boson mass is 120 GeV.

Smuons are produced in pairs through s-channel γ/Z exchange, selectrons and sneutrinos are pair produced through s-channel γ/Z exchange or t-channel $\tilde{\chi}_1^0$ and $\tilde{\chi}_1^\pm$ exchange respectively, see figure 1.

Benchmark point	P1 ($\sqrt{s} = 3$ TeV)	P2 ($\sqrt{s} = 1.4$ TeV)	
$\tilde{\chi}_1^0$ mass	340	357	GeV
$\tilde{\chi}_1^\pm, \tilde{\chi}_2^0$ mass	643, 643	487, 487	GeV
$\tilde{e}_R^\pm, \tilde{\mu}_R^\pm$ mass	1011, 1011	559, 559	GeV
$\tilde{e}_L^\pm, \tilde{\nu}_e$ mass	1100, 1097	650, 644	GeV
Br ($\tilde{\ell}_R^\pm \to \ell^\pm\ \tilde{\chi}_1^0$)	100	100	%
Br ($\tilde{e}_L \to e^-\ \tilde{\chi}_1^0$	16	19	%
Br ($\tilde{e}_L \to e^-\ \tilde{\chi}_2^0$)	29	28	%
Br ($\tilde{\nu}_e \to e^-\ \tilde{\chi}_1^+$)	56	53	%

Table 1. Benchmark parameters of the considered SUSY model.

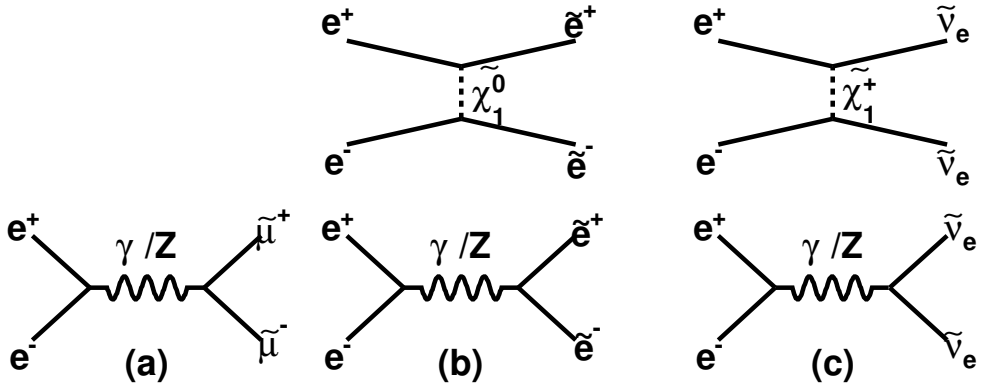

Figure 1. Slepton production diagrams: scalar muons (a), scalar electrons (b), and scalar neutrinos (c).

The cross sections, the decay modes, and the cross sections times the branching ratio of the signal processes are given in table 2. In the processes $e^+e^- \to \tilde{\ell}_R^+\tilde{\ell}_R^-$ each $\tilde{\ell}_R^\pm$ decays into an ordinary lepton and a $\tilde{\chi}_1^0$; the $\tilde{\chi}_1^0$ is stable and escapes detection due to its weakly interacting nature. Therefore, the experimental signature of these processes is two oppositely charged leptons plus missing energy. For the processes $e^+e^- \to \tilde{e}_L^+\tilde{e}_L^- \to e^+\ e^-\tilde{\chi}_2^0\ \tilde{\chi}_2^0$ and $e^+e^- \to \tilde{\nu}_e\tilde{\nu}_e \to e^+e^-\tilde{\chi}_1^+\tilde{\chi}_1^-$ the signature is an e^+e^-pair, four jets, and missing energy. Measuring the lepton energy distributions of these four processes allows the determination of their production cross sections and of the $\tilde{e}_R,\ \tilde{\mu}_R,\ \tilde{\nu}_e,\ \tilde{\chi}_1^\pm$, and $\tilde{\chi}_1^0$ masses. The aim of this study is to:

- Characterize the detector performance, namely lepton energy resolution, and boson mass resolution.

- Assess the statistical accuracy of the cross section measurements and the mass determination.

JHEP09(2013)001

$\sqrt{s}$ (TeV) Process	Decay Mode	3.0 σ (fb)	3.0 $\sigma \times Br$ (fb)	1.4 σ (fb)	1.4 $\sigma \times Br$ (fb)
$e^+e^- \to \tilde{\mu}^+_R\tilde{\mu}^-_R$	$\mu^+\mu^-\tilde{\chi}^0_1\tilde{\chi}^0_1$	0.70	0.70	1.53	1.53
$e^+e^- \to \tilde{e}^+_R\tilde{e}^-_R$	$e^+e^-\tilde{\chi}^0_1\tilde{\chi}^0_1$	6.10	6.10	5.91	5.91
$e^+e^- \to \tilde{e}^+_L\tilde{e}^-_L$	$e^+e^-\tilde{\chi}^0_2\tilde{\chi}^0_2 \to e^+e^-H/Z^0H/Z^0\tilde{\chi}^0_1\tilde{\chi}^0_1$	3.06	0.26	0.73	0.06
$e^+e^- \to \tilde{\nu}_e\tilde{\nu}_e$	$e^+e^-\tilde{\chi}^\pm_1\tilde{\chi}^\pm_1 \to e^+e^-W^+W^-\tilde{\chi}^0_1\tilde{\chi}^0_1$	13.7	4.30	5.37	1.51

Table 2. Signal processes, decay modes, cross sections, and cross sections times branching ratio ($\sigma \times Br$) at $\sqrt{s} = 3$ TeV and 1.4 TeV.

- Estimate the systematic errors, affecting the mass measurements, related to the event selection and the luminosity spectrum knowledge.
- Set the requirements for the detector time stamping capability and beam polarization.

The results presented in this article improve and supersede the previous results [6] obtained at 3 TeV only.

2 Event simulation

SUSY signal events and SM background events are generated using the WHIZARD program [7, 8], assuming zero polarisation of the electron and positron beams. WHIZARD is interfaced to Pythia 6.4 [9] for fragmentation and hadronization. For the generation of processes involving supersymmetric particles, the SUSY parameters are entered into WHIZARD using the Les Houches format [10]. The physics backgrounds simulated for this study are listed in table 3.

Beamstrahlung effects on the luminosity spectrum are included using results of the CLIC beam simulation for the CDR accelerator parameters [11]. There are three sources of the centre-of-mass energy spread: the momentum spread in the linac, the beamstrahlung which creates a long tail, and initial state radiation (ISR). The first two are collectively refererred to as "luminosity spectrum". The luminosity spectrum is obtained from the GuineaPig [12] beam simulation; it is used as input to WHIZARD in which initial state radiation and final state radiation (FSR) are enabled. Figure 2 shows the $\sqrt{s}$ distributions for the processes $e^+e^- \to \tilde{\mu}^+_R\tilde{\mu}^-_R$, at $\sqrt{s} = 3$ TeV and $e^+e^- \to \tilde{e}^+_R\tilde{e}^-_R$, at $\sqrt{s} = 1.4$ TeV. Integrated luminosities of 2000 fb^{-1} and 1500 fb^{-1} are assumed at 3.0 and 1.4 TeV respectively. At $\sqrt{s} = 3$ TeV an integrated luminosity of 2000 fb^{-1} corresponds to $\simeq$4 years (1 year = 10^7 s) of run at the nominal CLIC luminosity of 5.9×10^{34} cm^{-2}s^{-1}. At 1.4 TeV the nominal luminosity is 3.2×10^{34} cm^{-2}s^{-1}.

The physics background cross sections of the $e^+e^- \to \tilde{\ell}^+_R\tilde{\ell}^-_R$ processes are very large, see table 3. Taking into account the luminosity assumptions, the simulation and reconstruction of the background events would require very large computing and storage resources. To optimize the use of these resources preselection cuts are applied after generation of the

JHEP09(2013)001

$\sqrt{s}$ (TeV) Generator cuts Process	Decay mode	3.0 no $\sigma \times Br$ fb	3.0 yes $\sigma \times Br$ fb	1.4 no $\sigma \times Br$ fb	1.4 yes $\sigma \times Br$ fb
$e^+e^- \to \mu^+\mu^-$	$\mu^+\mu^-$	81.90	0.650	147.50	0.7200
$e^+e^- \to \mu^+\nu_e\mu^-\nu_e$	$\mu^+\mu^-$	65.60	3.500	44.70	2.1200
$e^+e^- \to \mu^+\nu_\mu\mu^-\nu_\mu$	$\mu^+\mu^-$	6.20	2.200	14.60	5.7300
$e^+e^- \to \mu^+\mu^-e^+e^-$	$\mu^+\mu^-$	1689.10	41.540	1608.00	23.8000
$e^+e^- \to \mathrm{W}^+\nu\mathrm{W}^-\nu$	$\mu^+\mu^-$	92.60	2.400	29.50	0.7300
$e^+e^- \to \mathrm{Z}^0\nu\mathrm{Z}^0\nu$	$\mu^+\mu^-$	40.50	0.002	10.80	0.0007
$e^+e^- \to$ All SUSY $-(\tilde{\mu}_R^+\tilde{\mu}_R^-)$	$\mu^+\mu^-$	0.31	0.310	0.12	0.1200
$e^+e^- \to e^+e^-$	e^+e^-	6226.00	77.100	21180.00	90.6000
$e^+e^- \to e^+\nu_e e^-\nu_e$	e^+e^-	179.30	91.100	200.80	96.4000
$e^+e^- \to W^+\nu W^-\nu$	e^+e^-	92.60	2.400	29.50	0.7300
$e^+e^- \to Z^0\nu Z^0\nu$	e^+e^-	40.50	0.002	10.80	0.0007
$e^+e^- \to$ All SUSY $-(\tilde{e}_R^+\tilde{e}_R^-)$	e^+e^-	1.04	1.040	1.77	1.7700
$e^+e^- \to W^+W^-Z^0$	$e^+e^-W^+W^-$	1.40	0.610	1.84	0.8400
$e^+e^- \to Z^0Z^0Z^0$	$e^+e^-Z^0Z^0$	0.50	0.023	0.75	0.0380
$e^+e^- \to$ All SUSY $-(\tilde{e}_L^+\tilde{e}_L^-, \tilde{\nu}_e\tilde{\nu}_e)$	$e^+e^-WW/HH/Z^0Z^0$	0.77	0.120	0.67	0.1000

Table 3. Background processes, decay modes and cross sections times branching ratio, $\sigma \times Br$, without and with preselection cuts, at 3 TeV and 1.4 TeV.

background events. The preselection requires two opposite charged leptons ($L1$ and $L2$) and the following conditions:

- $p_T(L1 \text{ and } L2) > 4\,\mathrm{GeV}$ and $10^\circ < \theta(L1 \text{ and } L2) < 170^\circ$
- $4^\circ < \Delta\phi(L1, L2) < 176^\circ$, $p_T(L1, L2) > 10\,\mathrm{GeV}$ and $M(L1, L2) > 100\,\mathrm{GeV}$

where p_T is the transverse momentum, θ the polar angle of the lepton, $\Delta\phi(L1, L2)$ the acoplanarity of the leptons, $p_T(\mathrm{L1}, \mathrm{L2})$ the vector sum of the p_T of the two leptons, and $M(\mathrm{L1}, \mathrm{L2})$ the invariant mass of the two leptons. Table 3 shows the decay modes, and the cross section times branching ratio values without and with preselection cuts. For the signal samples, these cuts are also applied after full simulation and reconstruction. The simulation is performed using the GEANT4-based [13] MOKKA program [14] with the CLIC_ILD_CDR detector geometry [15], which is based on the ILD detector concept [16] being developed for the ILC.

3 Event reconstruction

Events are subsequently reconstructed using the MARLIN reconstruction program [17]. The tracking systems of the CLIC detectors are designed to provide excellent momentum measurement for charged particle tracks. The track momenta and calorimeter data are input

JHEP09(2013)001

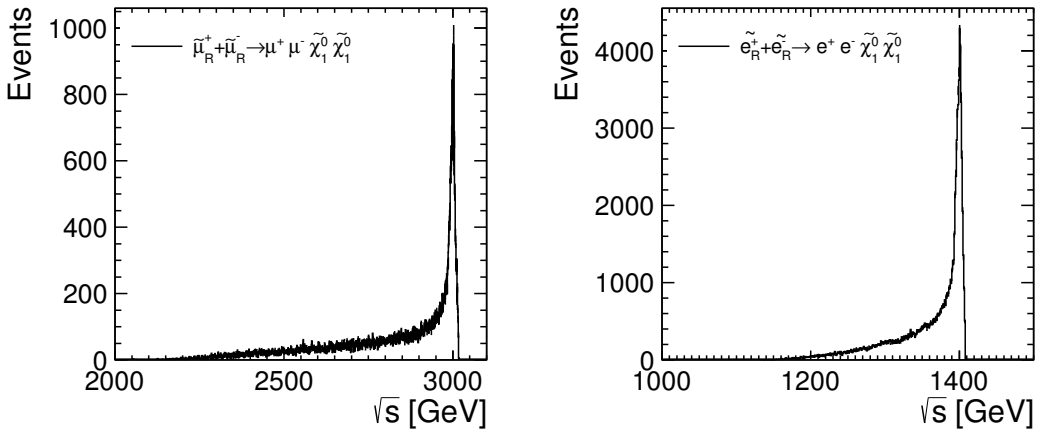

(a) $e^+e^- \to \tilde{\mu}_R^+\tilde{\mu}_R^-,\ \sqrt{s} = 3\,\text{TeV}$ (b) $e^+e^- \to \tilde{e}_R^+\tilde{e}_R^-,\ \sqrt{s} = 1.4\,\text{TeV}$

Figure 2. Centre-of-mass energy spectrum for the processes: $e^+e^- \to \tilde{\mu}_R^+\tilde{\mu}_R^-,\ \sqrt{s} = 3\,\text{TeV}$ (a), and $e^+e^- \to \tilde{e}_R^+\tilde{e}_R^-\,, \sqrt{s} = 1.4\,\text{TeV}$ (b).

to the PandoraPFA algorithm [18, 20] which performs particle flow objets (PFO) reconstruction, including particle identification and returns the best estimate for the momentum and energy of the particles.

3.1 Two lepton final states

The energy of the lepton is reconstructed from the momentum of the charged particle track and corrected for final state radiation and bremsstrahlung. The energy of photons and e^+e^- pairs from conversions within a cone of 20° around the reconstructed lepton direction is added to the energy from the track. Figure 3 shows, for the process $e^+e^- \to \tilde{e}_R^+\tilde{e}_R^-$, the true and reconstructed lepton energy distributions without (a) and with (b) photon radiation correction. For the process $e^+e^- \to \tilde{\mu}_R^+\tilde{\mu}_R^-$ the photon radiation corrections are much smaller. For both processes there is a good agreement between the true and reconstructed lepton energy distributions when photon radiation corrections are applied.

Table 4 shows the reconstruction efficiencies, ϵ_R, for the signal processes. For the process $e^+e^- \to \tilde{\ell}_R^+\tilde{\ell}_R^-$, ϵ_R is the number of good reconstructed lepton pairs divided by the number of generated lepton pairs. A lepton is considered as good when the reconstructed lepton matches the generated particle in space within 2°. For the process $e^+e^- \to \tilde{\mu}_R^+\tilde{\mu}_R^-$, at 3 TeV and 1.4 TeV, there is an inefficiency of about 2.5%; 2.0% is due to the cut on the lepton angle and 0.5% is coming from muon misidentification. For the process $e^+e^- \to \tilde{e}_R^+\tilde{e}_R^-$, at 3 TeV, there is an inefficiency of 6.5%; 4.0% is due to the cut on the lepton angle and 2.5% is coming from electron reconstruction or misidentification. At 1.4 TeV the inefficiency is 5.5%; 3.0% is due to the cut on the lepton angle and 2.5% is coming from electron reconstruction or misidentification.

The energy resolution is characterized using: $\Delta E/E^2_\text{True}$, where $\Delta E = E_\text{True} - E_\text{Reco}$, E_True is the lepton energy at generator level before final state radiation or bremsstrahlung, and E_Reco is the reconstructed lepton energy with photon radiation corrections.

JHEP09(2013)001

$\sqrt{s}$ (TeV) Process	Decay Mode	3 ϵ_R without $\gamma\gamma$	3 ϵ_R with $\gamma\gamma$	1.4 ϵ_R without $\gamma\gamma$	1.4 ϵ_R with $\gamma\gamma$
$e^+e^- \to \tilde{\mu}_R^+\tilde{\mu}_R^-$	$\mu^+\mu^-\tilde{\chi}_1^0\tilde{\chi}_1^0$	0.975	0.965	0.975	0.975
$e^+e^- \to \tilde{e}_R^+\tilde{e}_R^-$	$e^+e^-\tilde{\chi}_1^0\tilde{\chi}_1^0$	0.935	0.905	0.944	0.930
$e^+e^- \to \tilde{e}_L^+\tilde{e}_L^-$	$e^+e^-\tilde{\chi}_2^0\tilde{\chi}_2^0 \to e^+e^-H/Z^0H/Z^0\tilde{\chi}_1^0\tilde{\chi}_1^0$	0.66	0.63	0.61	0.57
$e^+e^- \to \tilde{\nu}_e\tilde{\nu}_e$	$e^+e^-\tilde{\chi}_1^\pm\tilde{\chi}_1^\pm \to e^+e^-W^+W^-\tilde{\chi}_1^0\tilde{\chi}_1^0$	0.49	0.46	0.43	0.40

Table 4. Reconstruction efficiency, ϵ_R, without and with $\gamma\gamma \to$ hadrons overlaid for the different signal processes, at $\sqrt{s} = 3\,\text{TeV}$ and 1.4 TeV. The statistical error on these efficiencies is $\sim 0.5\%$.

Figure 5 (a) and (b) show the lepton energy resolution, for the two lepton final state processes at $\sqrt{s} = 3\,\text{TeV}$ and without beam induced background, $\gamma\gamma \to$ hadrons. The resolution is parametrised using the sum of two Gaussian functions G1 and G2; G1 for the peak and G2 for the tails. For the muons the r.m.s. of G1 is $1.5 \cdot 10^{-5}\,\text{GeV}^{-1}$, and the r.m.s. of G2 is $4.9 \cdot 10^{-5}\,\text{GeV}^{-1}$. Only 4.1% of the events are outside of the central region; the central region of the distribution is defined within the interval $\Delta E/E^2_{\text{True}} = \pm 0.5 \cdot 10^{-3}\,\text{GeV}^{-1}$. The electron energy resolution is described by the Gaussian G1 with a very similar r.m.s. as that for muons, $1.4 \cdot 10^{-5}\,\text{GeV}^{-1}$, however, even with bremsstrahlung recovery, about 30% of the events are outside the central region. These are due to cases where final state radiation and bremsstrahlung are not sufficiently well accounted for; the tails are reasonably well described by the Gaussian G2 with r.m.s. $= 7.7 \cdot 10^{-5}\,\text{GeV}^{-1}$.

The SM process $e^+e^- \to \tau^+\tau^-$ is a potential background for the two leptons final state events. At 3 TeV the preselection cuts listed in section 2 reduce the $e^+e^- \to \tau^+\tau^- \to \mu^+\mu^-$ cross section from 252 fb to 0.05 fb. For 100 GeV particles the impact parameter resolution is 1.5 micron at 90 degree and 5 microns at 10 degree [22]. For the event selection, in addition to the preselection cuts, a cut on the impact parameter is applied. The cut value is 30 microns; it reduce the $\tau^+\tau^-$ cross section from 0.05 fb to 0.005 fb. This cross section is smaller than those of all other backgrounds listed in table 3 and represents less than 0.1% of all the backgrounds; this process was therefore considered as negligible. The same conclusion is reached for $e^+e^- \to \tau^+\tau^- \to e^+e-$ events and is valid at 1.4 TeV.

Hadronic final state events with semi-leptonic decays, e.g. $t\bar{t}$ events, are a potential background for two lepton final state events. To suppress these events, in addition to the preselection cuts described in section 2, a charged particle multiplicity cut is applied; the cut value is different at 3 TeV and 1.4 TeV. The selection efficiency of this cut, in presence of beam-induced background, is discussed in section 3.3.

3.2 Two leptons and four jets final states

For the processes $e^+e^- \to \tilde{e}_L^+\tilde{e}_L^-$ and $e^+e^- \to \tilde{\nu}_e\tilde{\nu}_e$, the parton topology signature required is two leptons and four quarks. After the reconstruction of all the particles in the event, the jet finder program FastJet [23] is used to reconstruct jets; the jet algorithm used is the inclusive anti-kt method. The choice of cylindrical coordinates is optimal since the background events originating from $\gamma\gamma \to$ hadrons interactions are forward boosted,

JHEP09(2013)001

similarly to the underlying events in pp collisions for which the anti-kt clustering has been optimised. The R parameter cut value is 1 and the minimum jet energy required is 20 GeV at $\sqrt{s} = 3$ TeV and 10 GeV at 1.4 TeV. An event is retained if six jets are found and if two of the jets are identified as isolated leptons. The lepton isolation criterion requires that the hadronic energy not associated to the lepton, in a cone of $\Delta R = 0.5$, normalized to the lepton energy is less than the value called "Ecut". The value "Ecut" is a function of the lepton energy and energy resolution.

Table 4 shows the reconstruction efficiencies of both processes, ϵ_{R} is the number of reconstructed six jet events, with two leptons, divided by the number of generated events with two leptons and four quarks. The efficiency includes the losses due to the lepton isolation requirement.

Figure 4 shows the electron energy distribution for the processes $e^+e^- \to \tilde{\nu}_e\tilde{\nu}_e$ (a) and $e^+e^- \to \tilde{e}_L^+\tilde{e}_L^-$ (b). There is good agreement between the true and reconstructed electron energy distributions when photon radiation corrections are applied.

For the processes with two electrons and four jets, see figure 5 (c) and (d), despite the presence of four jets, the electron energy resolution is consistent with the energy resolution obtained for the isolated electrons process, see figure 5 (b).

After event reconstruction and jet clustering the di-jet invariant masses of the 4 jets are computed. Out of the three possible combinations, the two di-jets with the smallest mass difference $\Delta M = M_{ij} - M_{kl}$ are retained; the boson mass is $M_B = (M_{ij} + M_{kl})/2$.

Other SM processes than those listed in table 3, namely $ZZ \to e^+e^-q\bar{q}$ and $e^+e^- \to t\bar{t} \to W^+W^-b\bar{b}$ events are potential backgrounds of the two leptons and four jets final states events. For ZZ events, at 3 TeV, the preselection cuts listed in section 2 reduce the ZZ cross section from 61.9 fb to 0.04 fb. For $t\bar{t}$ events in addition to the preselection cuts, a cut on the charged multiplicity reduces the $t\bar{t}$ cross section from 30.2 fb to 0.06 fb; this cut does not introduce any inefficiency on the signal event selection.

At 1.4 TeV, the preselection cuts listed in section 2 reduce the ZZ cross section from 142.7 fb to 0.09 fb. For $t\bar{t}$ events the preselection cuts and the charged particle multiplicity cut reduces the $t\bar{t}$ cross section from 137 fb to 0.6 fb. After event reconstruction and jet clustering the event selection requires two isolated leptons and four jets; this topological constraint is very effective in background reduction. At 3 TeV no ZZ and $t\bar{t}$ events are left when this selection is applied. At 1.4 TeV two $t\bar{t}$ events are left when this selection is applied.

3.3 Reconstruction with beam-induced Background

The creation of electron-positron pairs and the production of hadrons in $\gamma\gamma$ interactions are expected to be the dominating source of background events originating from the interaction region [21]. The beam-beam interaction leading to the production of these background particles was simulated with the GuineaPig program [12]. The average number of $\gamma\gamma$ interactions for each bunch crossing is 3.2 at 3 TeV and 1.3 at 1.4 TeV. At 3 TeV the pile-up of this background over the entire 156 ns bunch-train deposits 19 TeV of energy in the calorimeters, of which approximately 90% occurs in the endcap and 10% in the barrel

JHEP09(2013)001

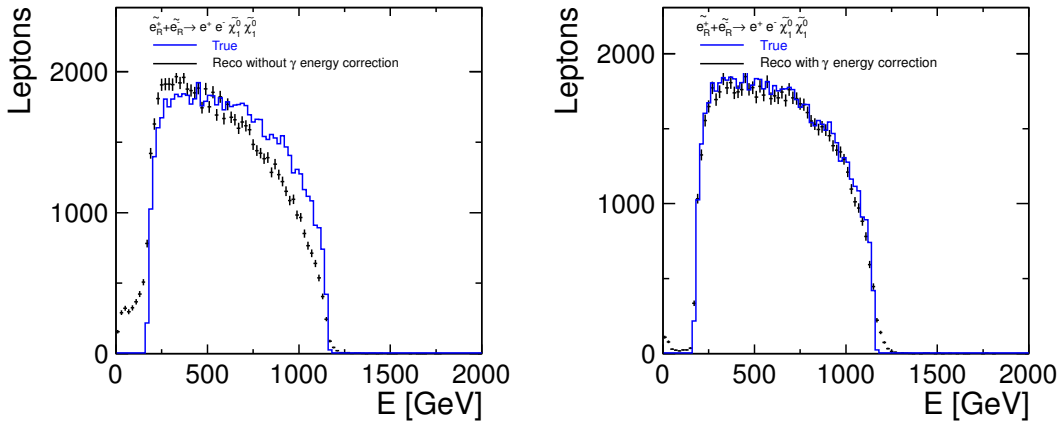

(a) Without photon energy correction (b) With photon energy correction

Figure 3. Process $e^+e^- \to \tilde{e}_R^+\tilde{e}_R^-$ at $\sqrt{s} = 3\,\text{TeV}$: true and reconstructed electron energy distributions, without (a), and with photon energy correction (b).

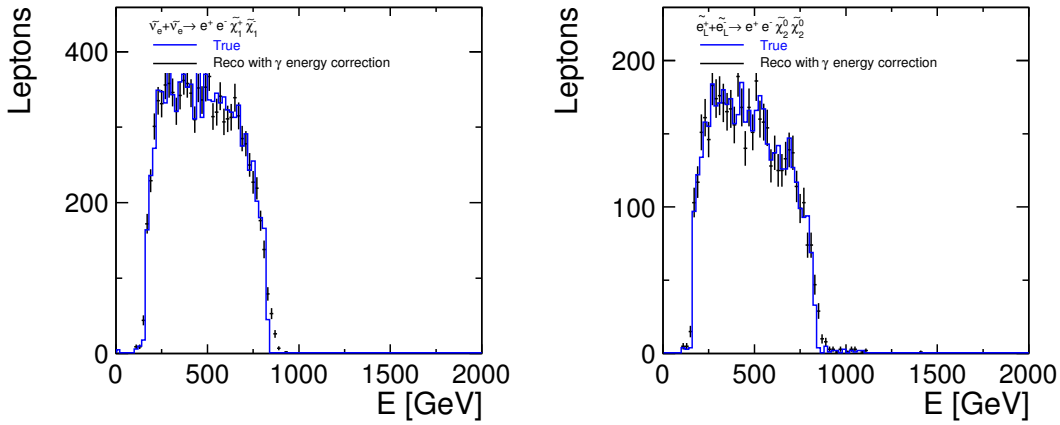

(a) $e^+e^- \to \tilde{\nu}_e^+\tilde{\nu}_e^-$ (b) $e^+e^- \to \tilde{e}_L^+\tilde{e}_L^-$

Figure 4. True and reconstructed electron energy distribution, with photon energy correction, for processes $e^+e^- \to \tilde{\nu}_e^+\tilde{\nu}_e^-$ (a), and $e^+e^- \to \tilde{e}_L^+\tilde{e}_L^-$ (b) at $\sqrt{s} = 3\,\text{TeV}$.

regions. On average, there is 1.2 TeV of reconstructed energy from $\gamma\gamma \to$ hadrons that are in the same readout window as the physics event.

At 3 TeV the mean energy and mean p_T of the particles originating from the $\gamma\gamma \to$ hadrons interactions is 1.6 GeV and 0.7 GeV respectively. To remove these particles two different methods are used.

For the two leptons final state events a cut on the p_T of the charged particles is applied. This selection removes most of the charged particles originating from $\gamma\gamma \to$ hadrons interactions. It preserves the lepton energy resolution as well as the charged particle multiplicity measurement necessary to suppress hadronic final state events with semi-leptonic decays.

JHEP09(2013)001

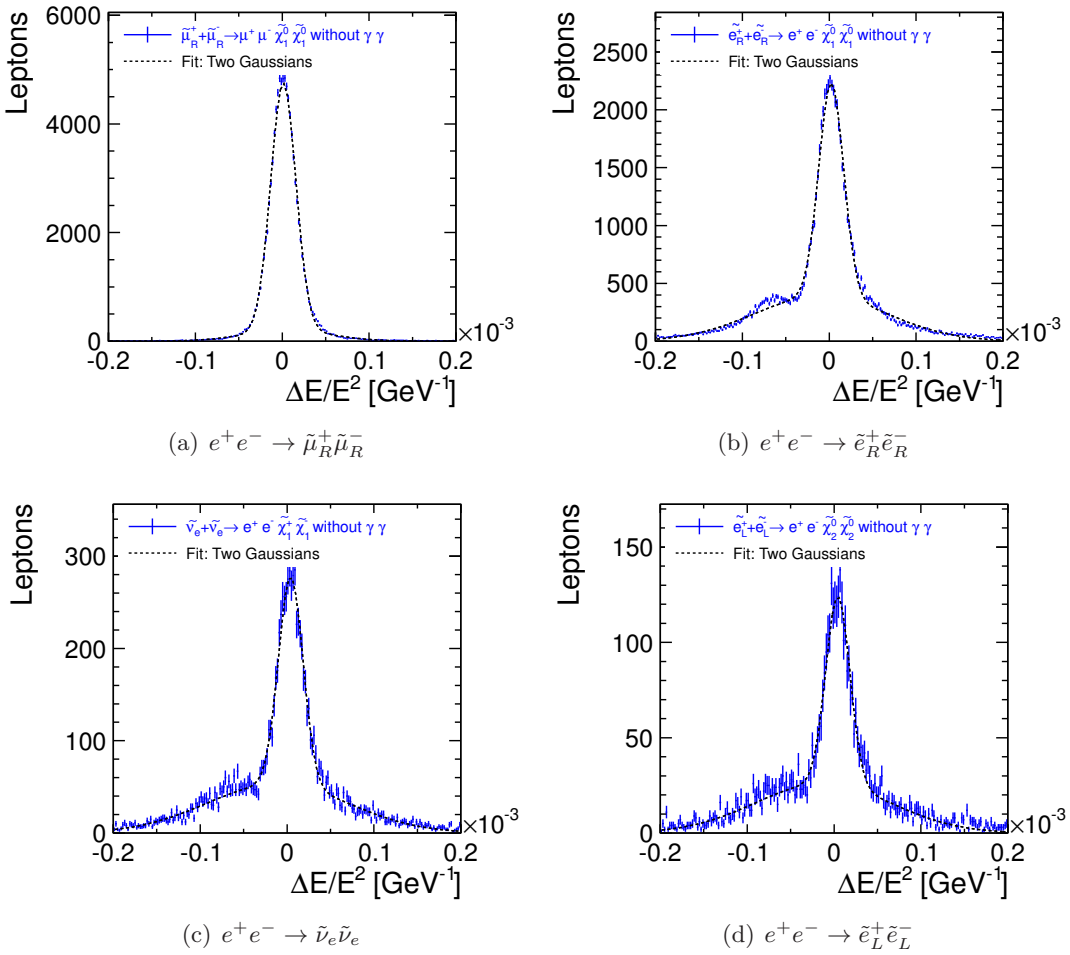

(a) $e^+e^- \to \tilde{\mu}_R^+\tilde{\mu}_R^-$ (b) $e^+e^- \to \tilde{e}_R^+\tilde{e}_R^-$

(c) $e^+e^- \to \tilde{\nu}_e\tilde{\nu}_e$ (d) $e^+e^- \to \tilde{e}_L^+\tilde{e}_L^-$

Figure 5. Lepton energy resolution, at $\sqrt{s} = 3\,\text{TeV}$, without $\gamma\gamma \to$ hadron background, for the processes: $e^+e^- \to \tilde{\mu}_R^+\tilde{\mu}_R^-$ (a), $e^+e^- \to \tilde{e}_R^+\tilde{e}_R^-$ (b), $e^+e^- \to \tilde{\nu}_e\tilde{\nu}_e$ (c), and $e^+e^- \to \tilde{e}_L^+\tilde{e}_L^-$ (d).

For the two leptons and four jets final state events, the particle flow object (PFO) selection, based on p_T cuts and timing cuts, is applied. This selection removes most of the charged and neutral particles originating from $\gamma\gamma \to$ hadrons interactions and reduces the background energy deposit. It preserves the jet energy resolution as well as the charged particle multiplicity measurement necessary to suppress hadronic final state events.

To investigate the effect of beam-induced background, the reconstruction software is run overlaying particles produced by $\gamma\gamma \to$ hadrons interactions [25]. The $\gamma\gamma \to$ hadrons event sample was generated with PYTHIA and simulated. From this sample we randomly select for each physics event the equivalent of 60 bunch crossings, assuming 3.2 events per bunch crossing at 3 TeV [21] and 1.3 events per bunch crossing at 1.4 TeV.

The detector hits from these events are merged with those from the physics event before the reconstruction. A time window of 10 nsec on the detector integration time is applied for all detectors, except for the HCAL barrel for which the window is 100 nsec. After particle reconstruction timing cuts in the range of 1 to 3 nsec are applied in order

JHEP09(2013)001

Photons		
Central region	1.0 GeV $< p_T <$ 4.0 GeV	t $<$ 2.0 nsec
cos$\theta \leq$ 0.975	0.2 GeV $\leq p_T <$ 1.0 GeV	t $<$ 1.0 nsec
Forward regions	1.0 GeV $< p_T <$ 4.0 GeV	t $<$ 2.0 nsec
cos$\theta >$ 0.975	0.2 GeV $\leq p_T <$ 1.0 GeV	t $<$ 1.0 nsec
Neutral hadrons		
Central region	1.0 GeV $< p_T <$ 8.0 GeV	t $<$ 2.5 nsec
cos$\theta \leq$ 0.975	0.5 GeV $\leq p_T <$ 1.0 GeV	t $<$ 1.5 nsec
Forward regions	1.0 GeV $< p_T <$ 8.0 GeV	t $<$ 1.5 nsec
cos$\theta >$ 0.975	0.5 GeV $\leq p_T <$ 1.0 GeV	t $<$ 1.0 nsec
Charged particles		
Central/Forward regions	1.0 GeV $< p_T <$ 4.0 GeV	t $<$ 2.0 nsec
	0.0 GeV $\leq p_T <$ 1.0 GeV	t $<$ 1.0 nsec

Table 5. Tight particle flow (PFO) selection cuts for the $\gamma\gamma \to$ hadron background suppression. The cut value depends on the particle id, on the detector region and on the p_T. The same cuts are used at $\sqrt{s} = 3$ TeV and $\sqrt{s} = 1.4$ TeV.

to reduce the number of particles coming from $\gamma\gamma \to$ hadrons interactions and to optimize the energy resolution. The cut values vary according to the particle type (photon, neutral hadron, charged particle), the detector region, (central, forward) and the p_T of the particle. Table 5 shows the cut values for the tight particle flow (PFO) selection. The presence of the $\gamma\gamma \to$ hadron background sets strong requirements for the design of the CLIC detector and its readout.

Figures 6 (a) and (b) show the lepton energy resolution, without and with $\gamma\gamma \to$ hadron background, for the processes $e^+e^- \to \tilde{\mu}_R^+\tilde{\mu}_R^-$ and $e^+e^- \to \tilde{e}_R^+\tilde{e}_R^-$ respectively. For these events a selection cut on the number of charged particles with $p_T > 4$ GeV is applied. The lepton energy resolution is preserved; the event selection efficiency is reduced by 1.0% for $e^+e^- \to \tilde{\mu}_R^+\tilde{\mu}_R^-$ and 3.3% for $e^+e^- \to \tilde{e}_R^+\tilde{e}_R^-$, see table 4. At 1.4 TeV the $\gamma\gamma \to$ hadron background is a factor two lower, no selection inefficiency is induced for the process $e^+e^- \to \tilde{\mu}_R^+\tilde{\mu}_R^-$; an inefficiency of 1.5% is induced for the process $e^+e^- \to \tilde{e}_R^+\tilde{e}_R^-$. In final states with four jets and two leptons, the background from $\gamma\gamma \to$hadrons cannot be removed using a similar p_T cut, as this would significantly degrade the jet energy reconstruction. Figure 6 (c) shows the bias in the reconstructed electron energy when the $\gamma\gamma \to$hadron background is included. This bias is due to additional background particles being associated with the electron in the attempt to account for FSR and bremsstrahlung. Without PFO cuts, the energy resolution is not degraded but the central value is shifted. Figure 6 (d) shows the lepton energy resolutions without and with $\gamma\gamma \to$ hadrons overlaid after tight PFO selection cuts. The cuts restore the central value and preserve the energy resolution, but reduce the reconstruction efficiency ϵ_R by 6%, see table 4. The efficiency includes the losses due to the lepton isolation requirement.

JHEP09(2013)001

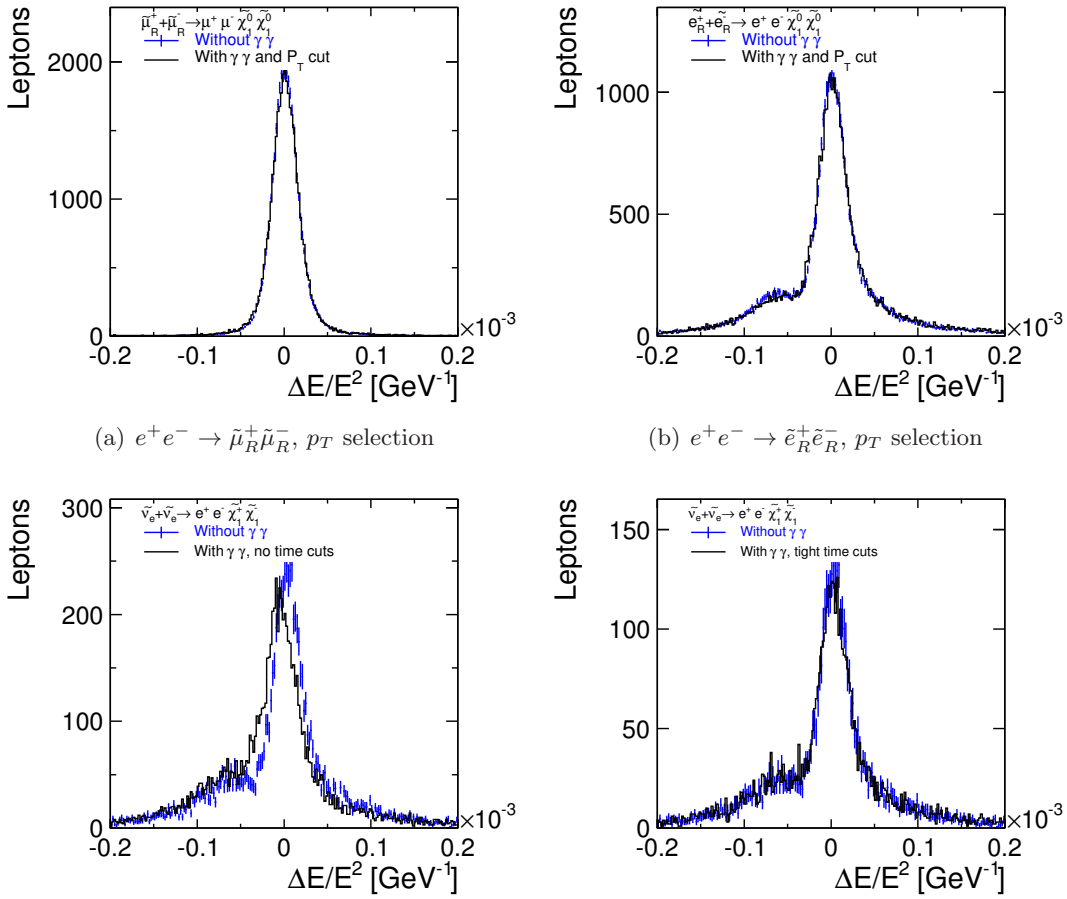

(a) $e^+e^- \to \tilde{\mu}_R^+\tilde{\mu}_R^-$, p_T selection

(b) $e^+e^- \to \tilde{e}_R^+\tilde{e}_R^-$, p_T selection

(c) $e^+e^- \to \tilde{\nu}_e\tilde{\nu}_e$, no PFO selection

(d) $e^+e^- \to \tilde{\nu}_e\tilde{\nu}_e$, tight PFO selection

Figure 6. Lepton energy resolution, without and with overlaid background at $\sqrt{s} = 3\,\text{TeV}$, for the processes: $e^+e^- \to \tilde{\mu}_R^+\tilde{\mu}_R^-$, $p_T > 4\,\text{GeV}$ selection (a), $e^+e^- \to \tilde{e}_R^+\tilde{e}_R^-$, $p_T > 4\,\text{GeV}$ selection (b), $e^+e^- \to \tilde{\nu}_e\tilde{\nu}_e$, no PFO selection (c), and $e^+e^- \to \tilde{\nu}_e\tilde{\nu}_e$, tight PFO selection (d).

Figure 7 shows, for the process $e^+e^- \to \tilde{\nu}_e\tilde{\nu}_e$ at 3 TeV, the W boson mass distribution without and with overlaid background: without PFO cuts (a) and with tight PFO selection cuts (b). The tight selection cuts give a similar mass distribution as the one obtained without overlaid background. To estimate the mass resolution degradation, figure 8 shows the W boson mass distribution fit, for the process $e^+e^- \to \tilde{\nu}_e\tilde{\nu}_e$ without overlaid background (a) and with overlaid background and tight selection cuts (b). The mass distributions are fitted with a Breit-Wigner convoluted with two Gaussians, one Gaussian takes into account the resolution in the peak, the second the tails. The most probable mass value is fixed as well as the natural width of the W. The width of the peak convoluted Gaussian is 4.1 GeV without overlaid background, it increases to 4.7 GeV with overlaid background and tight PFO selection cuts. The fraction of events in the peak gaussian is 90% without overlaid background and 89% with overlaid background.

JHEP09(2013)001

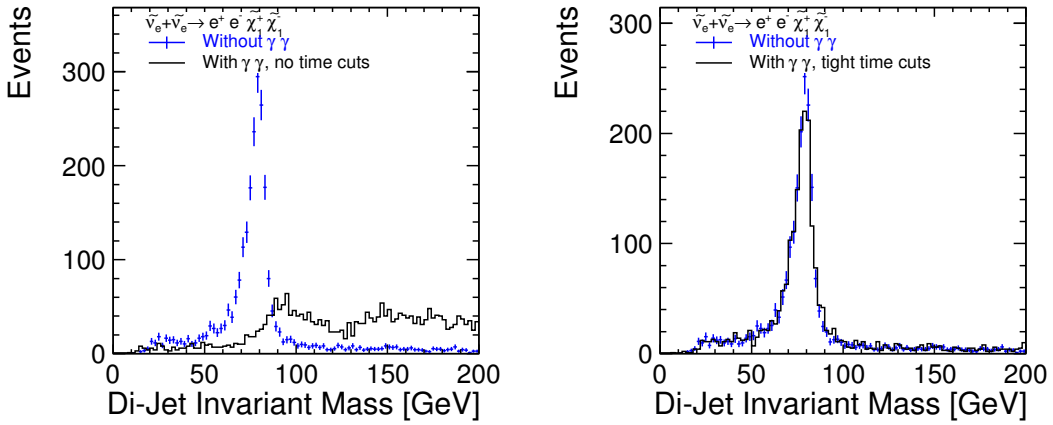

(a) No PFO selection cuts

(b) Tight PFO selection

Figure 7. W boson mass distribution, at $\sqrt{s} = 3\,\text{TeV}$, for the process $e^+e^- \to \tilde{\nu}_e\tilde{\nu}_e$ without and with overlaid background: without PFO cuts (a) and with tight PFO selection (b).

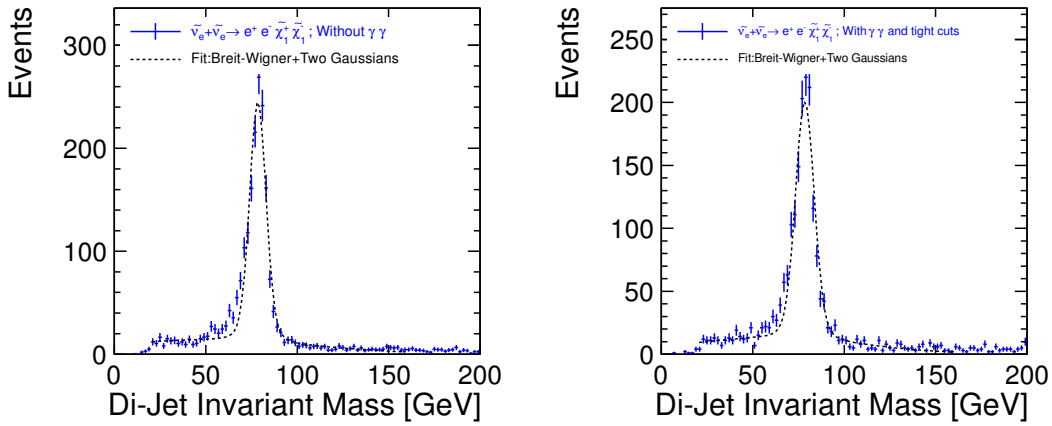

(a) Without overlaid background

(b) With overlaid background and tight selection cuts

Figure 8. W boson mass distribution fit, at $\sqrt{s} = 3\,\text{TeV}$, for the process $e^+e^- \to \tilde{\nu}_e\tilde{\nu}_e$ without overlaid background (a) and with overlaid background and tight selection cuts (b).

4 Event selection

All signal processes have two undetected $\tilde{\chi}_1^0$'s in the final state. Therefore, the main characteristics of these events are missing energy, missing transverse momentum and acoplanarity. Despite this signature, the large Standard Model backgrounds make the analysis rather challenging. After application of the lepton preselection cuts described in section 2 the following set of discriminating variables is used to distinguish signal events from background events:

- dilepton energy $E(L1) + E(L2)$,
- vector sum $p_T(L1, L2)$ of the two leptons,

JHEP09(2013)001

- algebraic sum $p_T(L1) + p_T(L2)$ of the two leptons,
- dilepton invariant mass $M(L1, L2)$,
- dilepton velocity $\beta(L1, L2)$,
- $\cos\theta(L1, L2)$; $\theta(L1, L2)$ is the polar angle of the vector sum of the two leptons,
- dilepton acollinearity $\pi - \theta_2 - \theta_1$,
- dilepton acoplanarity $\pi - \phi_2 - \phi_1$,
- dilepton energy imbalance $\Delta = |E(L1) - E(L2)|/|E(L1) + E(L2)|$,

where $L1$ and $L2$ are the two leptons. For illustration, figure 9 (a) shows for the process $e^+e^- \to \tilde{\mu}_R^+\tilde{\mu}_R^-$, the normalized distributions of some of the observables, for signal and background events, namely the dimuon energy, the vector sum of the p_T of the leptons, the algebraic sum of the p_T of the leptons the dimuon invariant mass, the acollinearity and the polar angle of the vector sum of the leptons.

The event selection proceeds as follows. The signal and background samples are split into two equal data size samples called "Monte Carlo" and "Data". The events of each sample are weighted such that the samples correspond to the same integrated luminosity. Then the Boosted Decision Trees (BDT) method from the multivariate analysis toolkit, TMVA [26], is used to implement the event selection. Firstly the discriminating variables of the Monte Carlo sample are input to the BDT method which trains the BDT probability classifier and computes the weights to distinguish signal from background. Next the weigths are used to the evaluate the "Data" sample and compute for each event a probability value used to rank the events to be signal or background-like. The cut value is chosen to optimise the significance $S_{MC}/\sqrt{S_{MC} + B_{MC}}$ versus the signal efficiency and the background rejection; S_{MC} and B_{MC} are the number of signal and background events of the MC sample. The cross section and the masses are determined after background subtraction and efficiency correction; the errors on the masses depend on $\sqrt{S_{data} + B_{data} + B_{MC}}$. A stronger BDT cut reduces slightly the significance but decreases significantly the errors on the masses. Figure 10 shows for the process $e^+e^- \to \tilde{e}_R^+\tilde{e}_R^-$ at $\sqrt{s} = 1.4$ TeV, the stacked electron energy distribution for signal and background events selected with a loose BDT classifier cut (a), and with an optimized BDT classifier cut (b). At 3 TeV the selection efficiency is 95% for the dimuon events, 90% for the dielectron events and 94% for the dielectron and four jet events. At 1.4 TeV the efficiency is 90% for the dimuon events, 80% for the dielectron events, and 90% for the dielectron and four jet events.

For the $\tilde{\nu}_e$ mass analysis, the event selection is done only with the BDT classifier cut; the boson mass is not used. The boson mass is only used for the $e^+e^- \to \tilde{e}_L^+\tilde{e}_L^-$ cross section determination; see the next section.

5 Slepton and gaugino mass determination

After the final selection, the slepton, neutralino or chargino masses are extracted from the position of the kinematic edges of the lepton energy distribution, a technique first proposed

JHEP09(2013)001

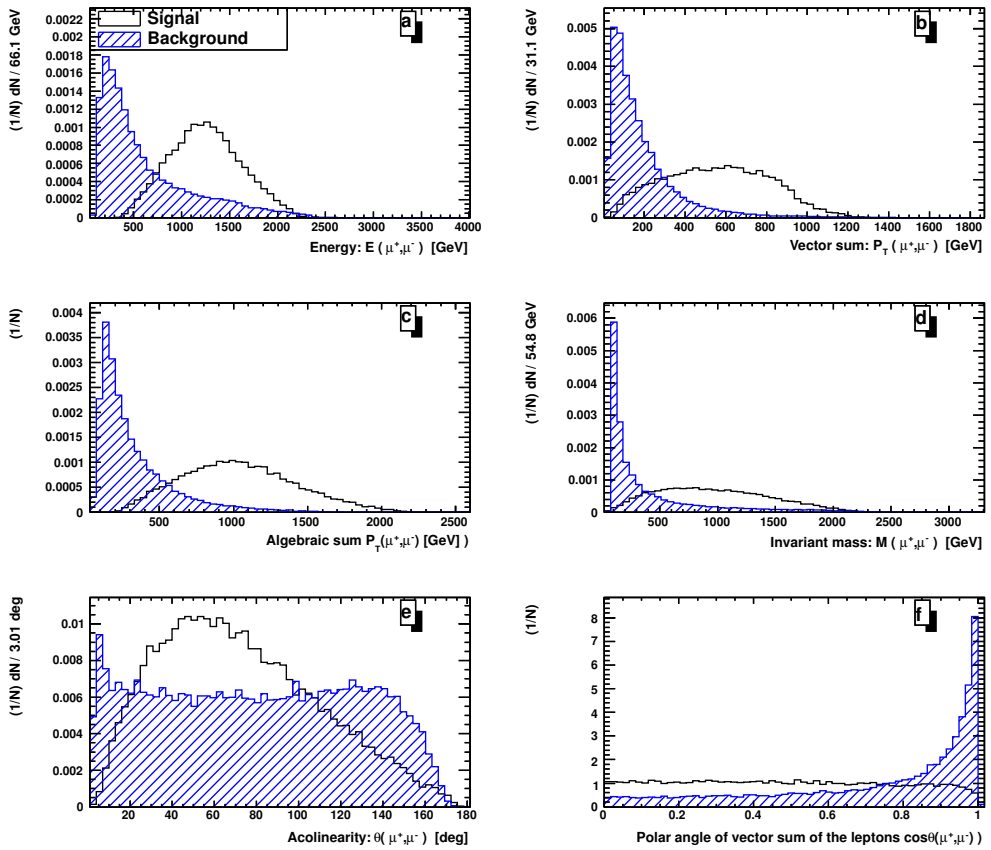

Figure 9. Discriminating variables used to separate signal and background events for the process $e^+e^- \to \tilde{\mu}_R^+\tilde{\mu}_R^-$ at $\sqrt{s} = 3\,\text{TeV}$: dimuon energy (a), dimuon p_T vector sum (b), dimuon p_T algebraic sum (c), dimuon invariant mass (d), acollinearity (e) and polar angle of the vector sum of the leptons (f).

for squarks [27], then extensively applied to sleptons [28]:

$$m_{\tilde{\ell}^\pm} = \frac{\sqrt{s}}{2}\left(1 - \frac{(E_H - E_L)^2}{(E_H + E_L)^2}\right)^{1/2} \quad \text{and} \quad m_{\tilde{\chi}_1^0} \text{ or } m_{\tilde{\chi}_1^\pm} = m_{\tilde{\ell}^\pm}\left(1 - \frac{2(E_H + E_L)}{\sqrt{s}}\right)^{1/2}, \tag{5.1}$$

where E_L and E_H are the low and high edges of the lepton energy distribution

$$E_{H,\,L} = \frac{\sqrt{s}}{4}\left(1 - \frac{m_{\tilde{\chi}_1^0}^2}{m_{\tilde{\ell}^\pm}^2}\right)\left(1 \pm \sqrt{1 - 4\frac{m_{\tilde{\ell}^\pm}^2}{s}}\right). \tag{5.2}$$

The masses are determined using a three-parameter fit to the background subtracted energy distribution, with $\sigma_{\tilde{\ell}^\pm}$, $m_{\tilde{\ell}^\pm}$, and $m_{\tilde{\chi}_1^0}$ or $m_{\tilde{\chi}_1^\pm}$ as parameters. The background subtraction is done using the "Monte Carlo" event sample used to train the classifier. The fit is performed with the MINUIT minimization package [29]. The fit function is:

$$f(E) = \int_{\sqrt{s_{\min}}}^{\sqrt{s_{\max}}} L_{\text{Eff}}(\sqrt{s}) \cdot \int_{E_L(\sqrt{s})}^{E_H(\sqrt{s})} U(\sigma_{\tilde{\ell}^\pm}, m_{\tilde{\ell}^\pm}, m_{\tilde{\chi}_1^0}, \sqrt{s}, \tau) \cdot D(E - \tau)\; d\sqrt{s}\; d\tau \tag{5.3}$$

JHEP09(2013)001

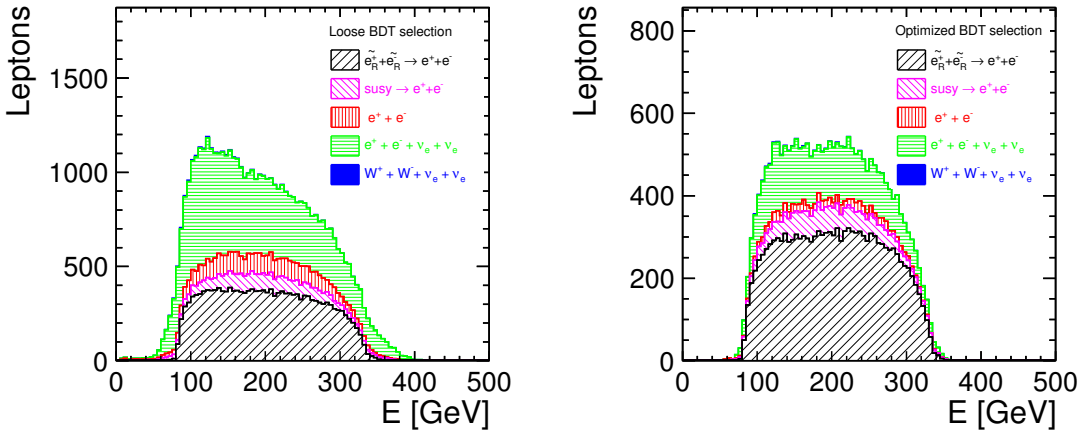

(a) Events selected with a loose BDT classifier cut

(b) Events selected with an optimized BDT classifier cut

Figure 10. Process $e^+e^- \to \tilde{e}_R^+\tilde{e}_R^-$ at $\sqrt{s} = 1.4\,\text{TeV}$: stacked electron energy distribution for signal and background events selected with a loose BDT classifier cut (a), and with an optimized BDT classifier cut (b).

$L_{\text{Eff}}(\sqrt{s})$ is the effective luminosity function, $L_{\text{Eff}}(\sqrt{s}) = L(\sqrt{s}) \otimes ISR(\sqrt{s}) \otimes \sigma_{\tilde{\ell}^\pm}(\sqrt{s})$. $L(\sqrt{s})$ is the luminosity spectrum prior to initial state radiation (ISR), $ISR(\sqrt{s})$ is the $\sqrt{s}$ variation due to ISR and $\sigma_{\tilde{\ell}^\pm}(\sqrt{s})$ is the slepton cross section. U is a uniform distribution of E, and depends on the process cross section $\sigma_{\tilde{\ell}^\pm}$, the slepton and gaugino masses and $\sqrt{s}$; the boundaries E_L, E_H of U are given by 5.2. D is the detector resolution function obtained from the fits shown in figure 5. Figure 11 shows, for the processes $e^+e^- \to \tilde{e}_R^+\tilde{e}_R^-$ (a) and $e^+e^- \to \tilde{\nu}_e\tilde{\nu}_e$ (b) at $\sqrt{s} = 3\,\text{TeV}$ the lepton energy distributions and fit results.

For the $\tilde{\nu}_e$ mass analysis, the event selection is done using the BDT optimized cut; the boson mass is not used. The mass is determined from the fit to the lepton energy distribution after background subtraction. Figure 12 (a) shows the stacked boson mass distribution of the signal $e^+e^- \to \tilde{\nu}_e\tilde{\nu}_e$ and background events selected with an optimized BDT classifier cut. The process $e^+e^- \to \tilde{e}_L^+\tilde{e}_L^-$ and other susy processes are the main backrounds; there is almost no SM background.

At 3 TeV, the cross section of the process $e^+e^- \to \tilde{e}_L^+\tilde{e}_L^-$ is too small to allow a simultaneous determination of the $\tilde{\nu}_e$ and $\tilde{e}_L^\pm$ masses, but the $e^+e^- \to \tilde{e}_L^+\tilde{e}_L^-$ cross section can be determined. Figure 12 (b) shows the stacked boson mass distribution of the signal and background events selected with a loose BDT classifier selection cut. Even with a loose selection cut there is almost no SM background. The process $e^+e^- \to \tilde{e}_L^+\tilde{e}_L^-$ is a background of the $e^+e^- \to \tilde{\nu}_e\tilde{\nu}_e$ process and vice versa. Despite the W peak the H final state events are clearly visible. The mass distribution of the Higgs boson is broader than the W one, due to a 5% background component from Z boson decays and due to the semi-leptonic heavy flavour decays in the $H \to b\bar{b}$ process.

To compute the $e^+e^- \to \tilde{e}_L^+\tilde{e}_L^-$ cross section two histograms are built. The first one with the events of the "data" sample selected with a loose BDT cut. The second with the events of the "MC" sample selected with a loose BDT cut; this sample does not comprise

JHEP09(2013)001

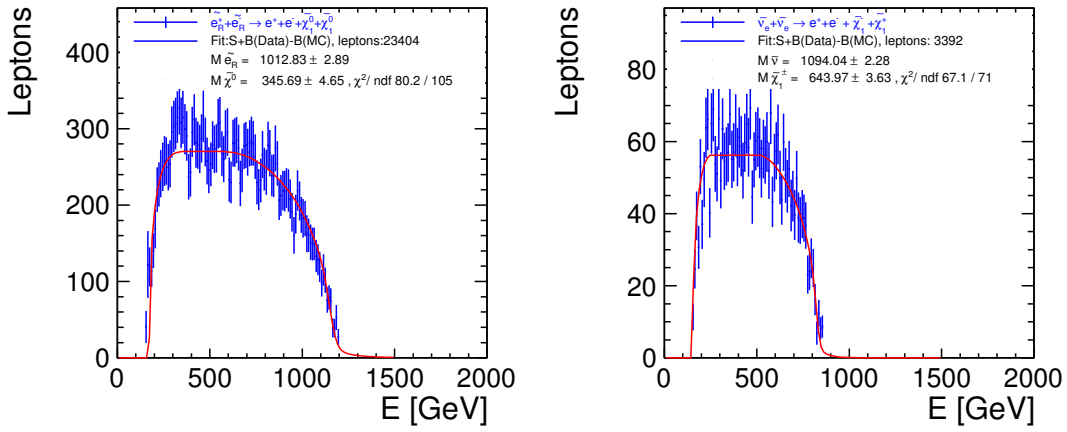

(a) $e^+e^- \to \tilde{e}_R^+\tilde{e}_R^-$ $\sqrt{s} = 3\,\text{TeV}$ (b) $e^+e^- \to \tilde{\nu}_e\tilde{\nu}_e$ $\sqrt{s} = 3\,\text{TeV}$

Figure 11. Lepton energy spectrum and fit results, for the processes: $e^+e^- \to \tilde{e}_R^+\tilde{e}_R^-$ (a) and $e^+e^- \to \tilde{\nu}_e\tilde{\nu}_e$ (b) at $\sqrt{s} = 3\,\text{TeV}$.

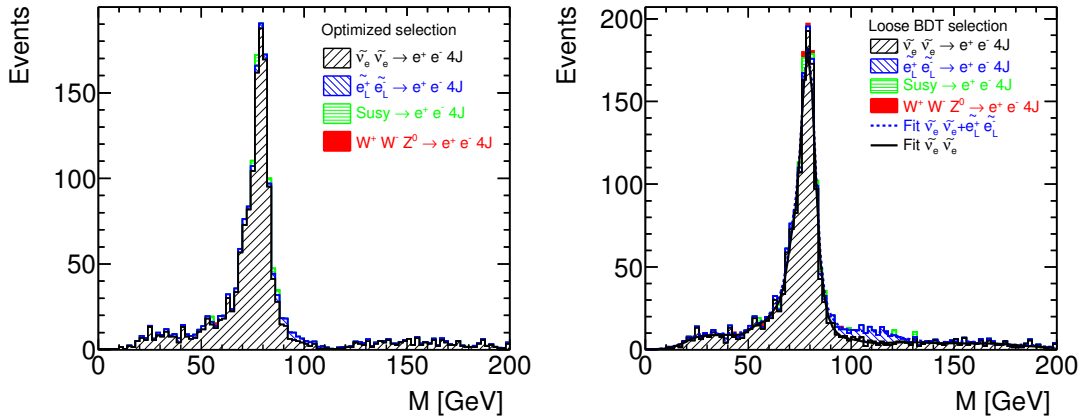

(a) Optimal BDT selection (b) Loose BDT selection

Figure 12. Process $e^+e^- \to \tilde{\nu}_e\tilde{\nu}_e$ at $\sqrt{s} = 3\,\text{TeV}$: stacked boson mass distribution for signal and background events selected with an optimized BDT classifier cut (a) and with loose BDT classifier cut (b).

$e^+e^- \to \tilde{e}_L^+\tilde{e}_L^-$. A fit to these distributions, the fit integral values over the mass region from 90 to 140 GeV, together with the efficiency corrections allow a determination of the $e^+e^- \to \tilde{e}_L^+\tilde{e}_L^-$ cross section. At 1.4 TeV, the cross section of the process $e^+e^- \to \tilde{e}_L^+\tilde{e}_L^-$ is too small to allow its determination.

Table 6 shows the values of the measured slepton cross sections, slepton masses, and gaugino masses at $\sqrt{s} = 3\,\text{TeV}$, assuming 2 ab^{-1} of integrated luminosity. Table 7 shows the results at 1.4 TeV, assuming 1.5 ab^{-1} of integrated luminosity.

JHEP09(2013)001

Process	Decay Mode	σ fb	$m_{\tilde{\ell}}$ GeV	$m_{\tilde{\chi}_1^0}$ or $m_{\tilde{\chi}_1^\pm}$ GeV
$e^+e^- \to \tilde{\mu}_R^+\tilde{\mu}_R^-$	$\mu^+\mu^-\tilde{\chi}_1^0\tilde{\chi}_1^0$	0.73 ± 0.02	1011.9 ± 4.9	342.7 ± 9.7
$e^+e^- \to \tilde{e}_R^+\tilde{e}_R^-$	$e^+e^-\tilde{\chi}_1^0\tilde{\chi}_1^0$	6.23 ± 0.04	1012.8 ± 2.9	345.7 ± 4.6
$e^+e^- \to \tilde{e}_L^+\tilde{e}_L^-$	$e^+e^-\tilde{\chi}_2^0\tilde{\chi}_2^0$	2.77 ± 0.20		
$e^+e^- \to \tilde{\nu}_e\tilde{\nu}_e$	$e^+e^-\tilde{\chi}_1^\pm\tilde{\chi}_1^\pm$	13.27 ± 0.23	1094.0 ± 2.3	644.0 ± 3.6

Table 6. Values of cross sections, slepton and gaugino masses, and statistical accuracies assuming an integrated luminosity of 2 ab^{-1} at $\sqrt{s} = 3\,\text{TeV}$.

Process	Decay Mode	σ fb	$m_{\tilde{\ell}}$ GeV	$m_{\tilde{\chi}_1^0}$ or $m_{\tilde{\chi}_1^\pm}$ GeV
$e^+e^- \to \tilde{\mu}_R^+\tilde{\mu}_R^-$	$\mu^+\mu^-\tilde{\chi}_1^0\tilde{\chi}_1^0$	1.51 ± 0.03	559.1 ± 0.4	357.1 ± 0.7
$e^+e^- \to \tilde{e}_R^+\tilde{e}_R^-$	$e^+e^-\tilde{\chi}_1^0\tilde{\chi}_1^0$	5.99 ± 0.05	557.9 ± 0.6	356.1 ± 0.9
$e^+e^- \to \tilde{\nu}_e\tilde{\nu}_e$	$e^+e^-\tilde{\chi}_1^\pm\tilde{\chi}_1^\pm$	5.13 ± 0.19	644.5 ± 2.2	488.8 ± 1.1

Table 7. Values of cross sections, slepton and gaugino masses, and statistical accuracies assuming an integrated luminosity of 1.5 ab^{-1} at $\sqrt{s} = 1.4\,\text{TeV}$.

6 Systematic uncertainty related to the event selection

For the event selection described in section 4 the signal sample, used to train the classifier to distinguish signal events from background events, was generated with the same slepton and gaugino masses as the data sample. With real data the masses are unknown. In this section we describe the procedure used to determine the masses and assess the error on the masses introduced when the MC masses are different from the true masses; the evaluation is done for the process $e^+e^- \to \tilde{\mu}_R^+\tilde{\mu}_R^-$ at 1.4 TeV.

Firstly signal events for lower smuon and neutralino masses are simulated and reconstructed; the smuon and neutralino masses are 459 GeV and 257 GeV respectively, that is to say, masses reduced by 100 GeV. These events are used to train the classifier. Figure 13 (a) shows the stacked muon energy distribution for signal and background events selected with the nine-variables classifier trained with masses lowered by 100 GeV, and with a loose selection cut. The energy distribution of the MC training sample is the red dash-dotted line; the energy distribution of the loose selected signal data sample is the black full line; and the energy distribution of the signal data sample without cut is the blue dashed line.

Next signal events for larger smuon and neutralino masses are simulated and reconstructed. The smuon and neutralino masses are 659 GeV and 457 GeV respectively, this is to say, masses increased by 100 GeV. These events are used to train the classifier which is then used to select the events. Figure 13 (b) shows the stacked muon energy distribution for signal and background events selected with the nine-variables classifier trained with masses increased by 100 GeV and with a loose selection cut.

JHEP09(2013)001

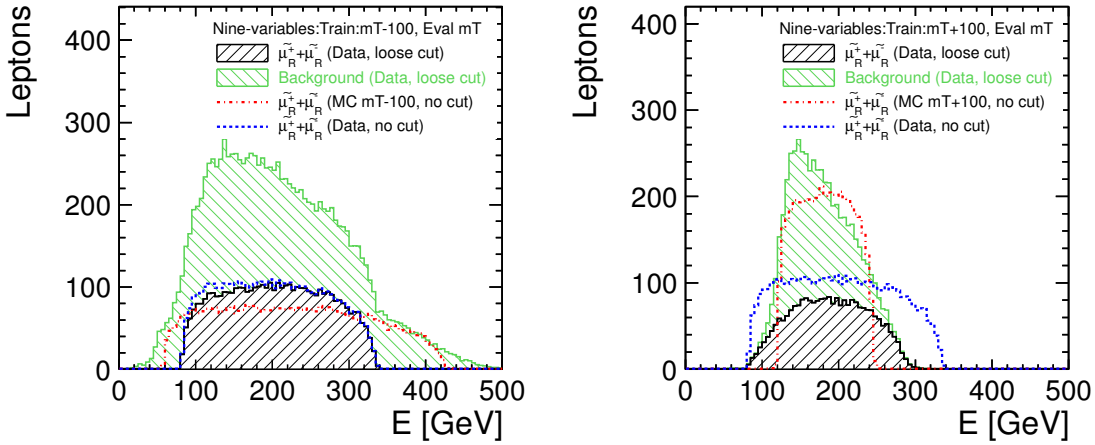

(a) Events selected with a nine-variables classifier trained with lower signal masses

(b) Events selected with a nine-variables classifier trained with larger signal masses

Figure 13. Process $e^+e^- \to \tilde{\mu}_R^+\tilde{\mu}_R^-$ at $\sqrt{s} = 1.4\,\text{TeV}$: stacked muon energy distribution for signal and background events selected with a nine-variables classifier trained with masses lowered by 100 GeV, and with a loose selection cut (a), and with a nine-variables classifier trained with masses increased by 100 GeV, and with a loose selection cut (b).

Despite a loose selection the signal energy distribution of the sample trained with larger masses is strongly biased; the end points have different values as those of the sample trained with lower masses. Among the nine variables, three are correlated with the energy of the leptons, namely the dilepton energy, velocity and energy imbalance; when the training value is far away from the true value, the end points are strongly affected and no rough end point determination is possible.

In a second step, these three variables are removed and a six-variables classifier is used to select the events. Figure 14 (a) shows the stacked muon energy distribution for signal and background events selected with the six-variables classifier trained with masses lowered by 100 GeV and with a loose selection cut.

Figure 14 (b) shows the stacked muon energy distribution for signal and background events selected with a classifier trained with masses increased by 100 GeV and with a loose selection cut. The signal energy distribution of the sample trained with larger masses is still biased, nevertheless the end points are visible and have similar values as those of the sample trained with lower masses. A rough estimation leads to E_L=80 GeV and E_H=340 GeV; with these values and $\sqrt{s}$=1.4 TeV formula 5.1 leads to a $\tilde{\mu}^{\pm}$ mass of 549.8 GeV and a $\tilde{\chi}_1^0$ mass of 347.7 GeV, these values are about 10 GeV lower than the true mass values.

These mass values are then used to simulate and reconstruct a new signal sample which is used to train the classifier with all nine variables. Figure 15 (a) shows the energy distribution of the data sample selected with the nine-variables classifier trained with masses lowered by 10 GeV and the fit result. Figure 15 (b) shows the energy distribution of the data sample selected with the nine-variables classifier trained with the true masses and the fit result. The smuon and neutralino masses determined after selection of the events with

JHEP09(2013)001

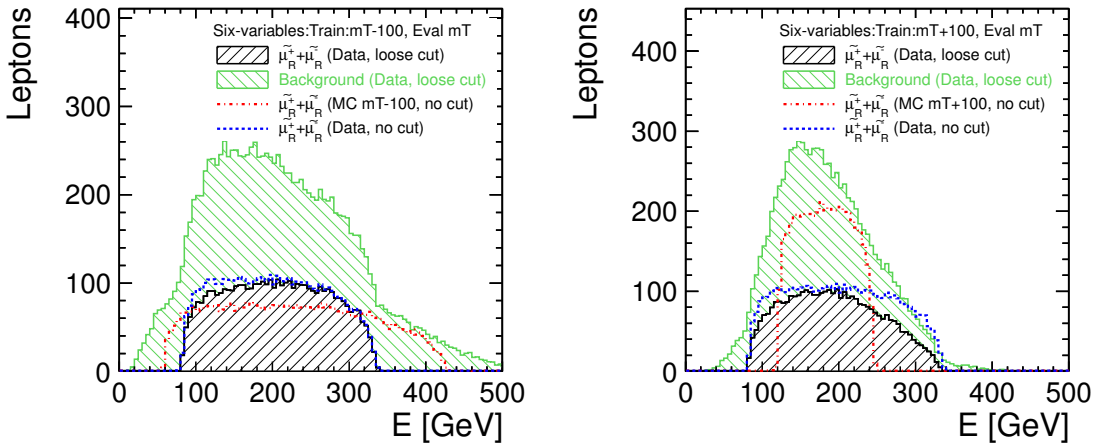

(a) Events selected with a six-variables classifier trained with lower signal masses

(b) Events selected with a six-variables classifier trained with larger signal masses

Figure 14. Process $e^+e^- \to \tilde{\mu}_R^+\tilde{\mu}_R^-$ at $\sqrt{s} = 1.4\,\text{TeV}$: stacked muon energy distribution for signal and background events selected with a six-variables classifier trained with masses lowered by 100 GeV, and with a loose selection cut (a), and with a six-variables classifier trained with masses increased by 100 GeV, and with a loose selection cut (b).

the classifier trained with masses lowered by 10 GeV are lower by 1.0 GeV and 1.3 GeV respectively; the values are statistically compatible.

7 Systematic uncertainty related to the luminosity spectrum

The beam energy is derived from the beam deflection measurement using high precision beam position monitors (BPM) pairs placed before and after the first dipole in the energy collimation section. This setup provides a relative energy resolution better than 0.04% [30]; therefore the impact on the slepton and gaugino masses is considered as negligible.

In this section the systematic uncertainty on the slepton and gaugino masses, related to uncertainties in the knowledge of the luminosity spectrum, is investigated. The assessment is done at 3.0 TeV where the beamstrahlung is largest. As can be seen from equation (5.3), the slepton and gaugino masses depend on the effective luminosity function $L_{\text{Eff}}(\sqrt{s}, \overrightarrow{p}) = L(\sqrt{s}, \overrightarrow{p}) \otimes ISR(\sqrt{s}) \otimes \sigma_{\tilde{\ell}^\pm}(\sqrt{s})$. The details about the method used to reconstruct the luminosity spectrum $L(\sqrt{s}, \overrightarrow{p})$ using Bhabha events are reported in [31]. The luminosity spectrum is parametrized with a function $F(x_1, x_2, \overrightarrow{p})$ where $x_{1,2} = 2E_{1,2}/\sqrt{s}$; $E_{1,2}$ is the energy of the e^+e^- particles before ISR; the vector $\overrightarrow{p}$ has 19 parameters. The model takes into account the longitudinal boost, the correlation between the two particle energies and accounts for asymmetric beams. A fit of $F(x_1, x_2, \overrightarrow{p})$ to the Bhabha events using the energy and the acollinearity of the outgoing e^+e^- particles allows the determination of the parameters $\overrightarrow{p}$ of the luminosity function and their errors. The parameters were determined at 3 TeV, using $2.2 \cdot 10^6$ events and taking into account the e^+e^- energy resolution.

JHEP09(2013)001

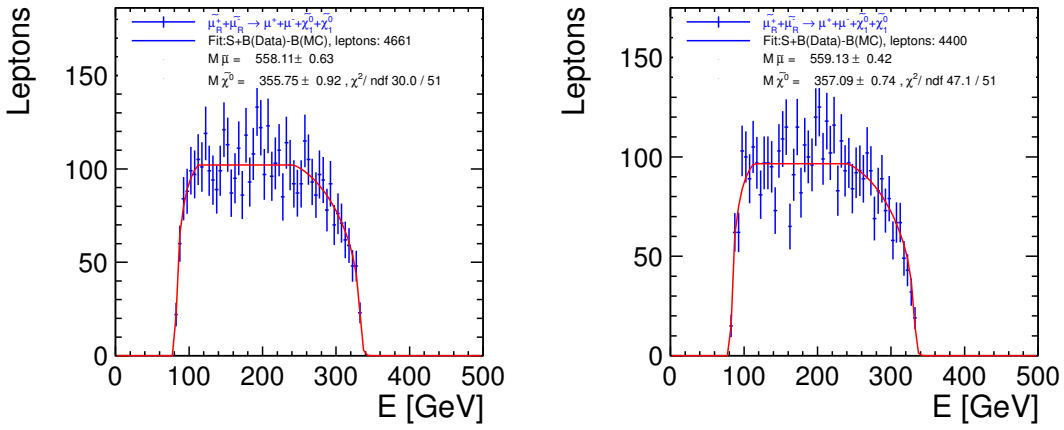

(a) Events selected with a classifier trained with signal masses lowered by 10 GeV

(b) Events selected with a classifier trained with the true signal masses

Figure 15. Process $e^+e^- \to \tilde{\mu}_R^+\tilde{\mu}_R^-$ at $\sqrt{s} = 1.4\,\text{TeV}$: muon energy distribution and fit results for events selected with a nine-variables classifier trained with signal masses lowered by 10 GeV (a), for events selected with a nine-variables classifier trained with the true signal masses (b).

To estimate the systematic error on the masses due to the luminosity spectrum, the mass fit is performed 38 times. Prior to each fit the effective luminosity spectrum $L_{\text{Eff}}(\sqrt{s}, \overrightarrow{p})$ is computed; one parameter p_i is changed to $p_i + \frac{\sigma_{p_i}}{2}$ or $p_i - \frac{\sigma_{p_i}}{2}$ and all other parameters are kept to their nominal value.

The error on the mass from the luminosity is:

$$\sigma_m = \sqrt{\sum_{i,j} \delta_i C_{ij} \delta_j} \tag{7.1}$$

C_{ij} is the correlation matrix obtained from the luminosity spectrum fit and:

$$\delta_i = m(L_{\text{Eff}}(\sqrt{s}, \overrightarrow{p} + \overrightarrow{e}_i \frac{\sigma_{p_i}}{2})) - m(L_{\text{Eff}}(\sqrt{s}, \overrightarrow{p} - \overrightarrow{e}_i \frac{\sigma_{p_i}}{2})). \tag{7.2}$$

where m is the result of the mass fit described in section 5.

Table 8 shows the values of the slepton and gaugino masses, the corresponding statistical uncertainty, and the systematic errors from the knowledge of the shape of the luminosity spectrum. For 2 ab^{-1} of integrated luminosity, the statistical errors are dominant.

8 Polarization

Beam polarization is very helpful in the study of SUSY processes both to improve the signal-to-background ratio and as an analyzer [32], in particular to establish the chirality of the sleptons. different electron and positron beam polarization conditions. Running with left polarized electron beam would establish the chirality of the selectron which decays into two leptons and of the selectron and sneutrinos which decay into two leptons and four jets. Running with right polarized electron beam would increase the cross sections of the $\tilde{\ell}_R$ processes and reduce some of the backgrounds.

JHEP09(2013)001

Process	$m_{\tilde{\ell}}$ GeV	σ_m (stat)%	σ_m (lumi)%	$m_{\tilde{\chi}_1^0}$ or $m_{\tilde{\chi}_1^\pm}$ GeV	σ_m (stat)%	σ_m (lumi)%
$e^+e^- \to \tilde{\mu}_R^+\tilde{\mu}_R^-$	1011.9	0.48	0.02	342.7	2.8	0.06
$e^+e^- \to \tilde{e}_R^+\tilde{e}_R^-$	1012.8	0.28	0.02	345.7	1.3	0.06
$e^+e^- \to \tilde{\nu}_e\tilde{\nu}_e$	1094.0	0.21	0.02	644.0	0.56	0.03

Table 8. Slepton and gaugino masses, statistical and systematic uncertainties from the knowledge of the shape of the luminosity spectrum (lumi) ,at $\sqrt{s} = 3\,\text{TeV}$.

Process	$e^+e^- \to \tilde{\mu}_R^+\tilde{\mu}_R^-$ $\sigma(fb)$	$e^+e^- \to \tilde{e}_R^+\tilde{e}_R^-$ $\sigma(fb)$	$e^+e^- \to \tilde{e}_L^+\tilde{e}_L^-$ $\sigma(fb)$	$e^+e^- \to \tilde{\nu}_e\tilde{\nu}_e$ $\sigma(fb)$
beam polarization				
e^- : none , e^+ :none	0.72	6.05	3.06	13.76
e^- : L80%, e^+ :none	0.46	2.59	4.78	21.90
e^- : R80%, e^+ :none	0.98	9.51	1.34	5.62
e^- : R80%, e^+ :L60%	1.15	11.40	1.14	4.56

Table 9. Signal processes cross sections (σ), for different electron, positron beam polarization conditions, at $\sqrt{s} = 3\,\text{TeV}$.

9 Summary

The accuracy of the slepton and gaugino mass determination and of the process cross section measurement in pair produced $\tilde{e}_R, \tilde{e}_L, \tilde{\mu}_R$, and $\tilde{\nu}_e$ processes has been studied at CLIC with the CLIC_ILD_CDR detector model for two specific SUSY benchmark scenarios at $\sqrt{s} = 3\,\text{TeV}$ and $1.4\,\text{TeV}$. The analysis is based on two lepton and two lepton plus four jet final states.

The electron and muon energy resolution and the boson mass resolution are not affected by the beam induced background, provided the detectors have timing capabilities of the order of 1 nsec allowing for the application of PFO selection cuts. The reconstructed boson mass resolution allows the distinction of the final states of $W^\pm$ and light H; b tagging improves the purity of the $W^\pm$ and H samples.

Slepton cross sections, slepton and gaugino masses can be extracted from the lepton energy distributions. At 3.0 TeV, for 2.0 ab^{-1} of integrated luminosity the relative statistical error on the masses is in the range of 0.2% to 0.5% for the sleptons and in the range of 0.6% to 2.8% for the gauginos. At 1.4 TeV, for 1.5 ab^{-1} of integrated luminosity, the relative statistical errors, on the slepton and gaugino masses are in the range of 0.1% to 0.3%.

A major source of smearing of the kinematic edges of the lepton energy spectrum is beamstrahlung and ISR. The measurement of the luminosity spectrum with Bhabha events, allows a good control of the beamstrahlung. The systematic errors on the slepton and gauginos masses due to the knowledge of the luminosity spectrum were estimated.

JHEP09(2013)001

At 3.0 TeV for 2.0 ab^{-1} of integrated luminosity the statistical errors are larger than the systematic errors.

The work presented in this paper has been carried out in the framework of the CLIC detector and physics study.

Acknowledgments

We are grateful to the colleagues who contributed to this study. Daniel Schulte for making available the beam spectrum and the $\gamma\gamma \to$ hadron background events. D.Schlatter and A.Lucaci-Timoce for a thorough reading of the manuscript.

References

[1] Y. Golfand and E. Likhtman, *Extension of the algebra of Poincaré group generators and violation of p invariance*, *JETP Lett.* **13** (1971) 323 [INSPIRE].

[2] D.V. Volkhov and V.P. Akulov, *Is the neutrino a goldstone particle?*, *Phys. Lett.* **B 46** (1973) 109 [INSPIRE].

[3] J. Wess and B. Zumino, *Supergauge transformations in four-dimensions*, *Nucl. Phys.* **B 70** (1974) 39 [INSPIRE].

[4] P. Fayet and S. Ferrara, *Supersymmetry*, *Phys. Rept.* **32** (1977) 249 [INSPIRE].

[5] A. Salam and J. Strathdee, *Supersymmetry and superfields*, *Fortschr. Phys.* **26** (1978) 57 [INSPIRE].

[6] J.-J. Blaising et al., *Physics performances for scalar electrons, scalar muons and scalar neutrinos searches at CLIC*, arXiv:1201.2092 [INSPIRE].

[7] W. Kilian, T. Ohl and J. Reuter, *WHIZARD: simulating multi-particle processes at LHC and ILC*, *Eur. Phys. J.* **C 71** (2011) 1742 [arXiv:0708.4233] [INSPIRE].

[8] M. Moretti et al., *O'Mega : an optimizing matrix element generator*, LC-TOOL-2001-040 (2001).

[9] T. Sjöstrand, S. Mrenna and P.Z. Skands, *PYTHIA 6.4 physics and manual*, *JHEP* **05** (2006) 026 [hep-ph/0603175] [INSPIRE].

[10] J. Alwall et al., *A standard format for Les Houches event files*, *Comput. Phys. Commun.* **176** (2007) 300 [hep-ph/0609017] [INSPIRE].

[11] CLIC Study Team, H. Braun et al., *CLIC 2008 parameters*, CLIC-NOTE-764 (2008).

[12] D. Schulte, *Study of electromagnetic and hadronic background in the interaction region of the TESLA collider*, TESLA-97-08 (1997).

[13] GEANT4 collaboration, S. Agostinelli et al., *GEANT4: a simulation toolkit*, *Nucl. Instrum. Meth.* **A 506** (2003) 250 [INSPIRE].

JHEP09(2013)001

[14] P. Mora de Freitas, *Mokka, main guidelines and future*, in the proceedings of the *International Conference on Linear Colliders (LCWS 04)*, April 19–23, Paris, France (2004).

[15] A. Münnich and A. Sailer, *The CLIC ILD CDR geometry for the CDR Monte Carlo mass production*, LCD-Note-2011-002 (2011).

[16] ILD Concept Group — Linear Collider collaboration, T. Abe et al., *The international large detector: letter of intent*, arXiv:1006.3396 [INSPIRE].

[17] F. Gaede, *Marlin and LCCD: software tools for the ILC*, *Nucl. Instrum. Meth.* **A 559** (2006) 177 [INSPIRE].

[18] M.A. Thomson, *Particle flow calorimetry and the PandoraPFA algorithm*, *Nucl. Instrum. Meth.* **A 611** (2009) 25 [arXiv:0907.3577] [INSPIRE].

[19] N. Alster and M. Battaglia, *Determination of Chargino and Neutralino Masses in high-mass SUSY scenarios at CLIC*, LCD-Note-2011-003 (2011).

[20] J. Marshall, A. Münnich and M. Thomson, *Performance of particle flow calorimetry at CLIC*, *Nucl. Instrum. Meth.* **A 700** (2013) 153 [arXiv:1209.4039] [INSPIRE].

[21] T. Barklow et al., *Simulation of $\gamma\gamma \to$ hadrons background at CLIC*, LCD-Note-2011-020 (2011).

[22] L. Linssen et al., *Physics and detectors at CLIC : CLIC conceptual design report*, ANL-HEP-TR-12-01 (2012).

[23] M. Cacciari and G.P. Salam, *Dispelling the N^3 myth for the k_t jet-finder*, *Phys. Lett.* **B 641** (2006) 57 [hep-ph/0512210] [INSPIRE].

[24] M. Battaglia and P. Ferrari, *A study of $e^+e^- \to H^0A^0 \to b\bar{b}b\bar{b}$ at 3 TeV at CLIC*, LCD-Note-2010-006 (2010).

[25] P. Schade and A. Lucaci-Timoce, *Description of the signal and background event mixing as implemented in the Marlin proceSSOR OverlayTiming*, LCD-Note-2011-006 (2011).

[26] A. Hocker et al., *TMVA — Toolkit for Multivariate Data Analysis*, PoS(ACAT)040 [physics/0703039] [INSPIRE].

[27] J.L. Feng and D.E. Finnell, *Squark mass determination at the next generation of linear e^+e^- colliders*, *Phys. Rev.* **D 49** (1994) 2369 [hep-ph/9310211] [INSPIRE].

[28] H.-U. Martyn and G.A. Blair, *Determination of sparticle masses and SUSY parameters*, hep-ph/9910416 [INSPIRE].

[29] F. James and M. Roos, *Minuit: a system for function minimization and analysis of the parameter errors and correlations*, *Comput. Phys. Commun.* **10** (1975) 343 [INSPIRE].

[30] M. Aicheler et al., *A multi-TeV linear collider based on CLIC technology: CLIC conceptual design report*, CERN-2012-007 (2012).

[31] A, Sailer and S. Poss, *Differential luminosity measurement using Bhabha events*, CERN-LCD-Note-2011-040 (2011).

[32] G. Moortgat-Pick et al., *The role of polarized positrons and electrons in revealing fundamental interactions at the linear collider*, *Phys. Rept.* **460** (2008) 131 [hep-ph/0507011] [INSPIRE].

JHEP09(2013)001